

# Temporal pulse response of quasi-periodic Fibonacci Fabry–Perot type optical filters

E. COJOCARU

Department of Lasers, National Institute of Laser, Plasma and Radiation Physics, P.O. Box MG–36, Bucharest–Magurele, R–76900 Romania.

A specific behaviour of quasi-periodic multilayers is the existence of isolated peaks inside the forbidden transmission gap. Thus, quasi-periodic multilayers may be an alternative to the periodic structures with defects. The compressing capacity of quasi-periodic Cantor filters has been presented by other authors. We analyse comparatively the compressing capacity of quasi-periodic Fibonacci (F) and Fibonacci Fabry–Perot (FFP) multilayers at normal incidence. Various pairs of nondispersive layer refractive indices and different embedding media are considered. Symmetrical FFP multilayers admit wider ranges of layer refractive indices at which parameters characterising the compressing capacity attain certain levels.

## 1. Introduction

During the past few years there has been observed a growing interest in the quasi-periodic dielectric structures. They fall between the complete perfect periodic and the random or disordered structures. Cantor and Fibonacci quasi-periodic fractal structures have been studied theoretically and experimentally [1]–[6]. The interest in these fractal structures is both for basic physics and for applications. A specific behaviour of the transmission spectrum from these quasi-periodic structures is the existence of isolated peaks inside the forbidden gap. Thus, a quasi-periodic multilayer may be an alternative to the periodic structure with defects [7], [8]. Recently, GARZIA *et al.* [9] analysed the temporal pulse response of a Cantor fractal structure and they put in evidence the compression of an input Gaussian temporal pulse.

In this paper, an analysis of the compressing capacity of Fibonacci (F) and Fibonacci Fabry–Perot (FFP) filters at normal incidence is given. The optimal situation is considered when the frequency spectrum of the Gaussian input pulse, which is centred in the middle of the forbidden gap, is wide enough to cover the isolated peaks existing inside the gap. Various pairs of nondispersive layer refractive indices and different embedding media are considered. The usual transfer matrix formalism is applied [10].

Throughout the paper all regions are assumed to be linear, homogeneous, nonabsorbing, and with no optical activity.

## 2. Fibonacci and Fibonacci Fabry-Perot sequences

A binary sequence  $F$  is constructed recursively [6]:  $S_k = \{S_{k-2}S_{k-1}\}$ , for  $k \geq 2$ , with  $S_0 = \{b\}$  and  $S_1 = \{a\}$ . It follows that  $S_2 = \{ba\}$ ,  $S_3 = \{aba\}$ ,  $S_4 = \{baaba\}$ , etc. Thus, for  $k \geq 2$ , the sequence  $S_k$  is generated by transformations  $a \rightarrow ba$ ,  $b \rightarrow a$ . If we apply transformations  $a \rightarrow ab$ ,  $b \rightarrow a$ , the sequence  $S'_k$  is generated recursively:  $S'_k = \{S'_{k-1}S'_{k-2}\}$ , for  $k \geq 2$ , with  $S'_0 = S_0 = \{b\}$  and  $S'_1 = S_1 = \{a\}$ . It follows that  $S'_2 = \{ab\}$ ,  $S'_3 = \{aba\}$ ,  $S'_4 = \{abaab\}$ , etc. Consider that  $a$  and  $b$  are two dielectric layers of optical thickness  $L$  and refractive indices  $n_1$  and  $n_2$ , respectively, with  $n_1 < n_2$ . Note that  $L$  is expressed in terms of a reference wavelength  $\lambda_0$ , e.g., for quarterwave-thick layers  $L = \lambda_0/4$ . For a given stage  $k$ , both  $S_k$  and  $S'_k$  have the same complex amplitude transmission coefficient  $t_k$ . Thus, we consider both of them as case A. An illustration of sequences  $S_k$  and  $S'_k$  is given in Fig. 1 (see the first two sequences from the upper side) at stage  $k = 7$ . The line  $OO'$  indicates the beginning of the sequence. The difquasi-periodiciference between sequences  $S_k$  and  $S'_k$  is that, at various stages  $k$ , the light travelling from the left to the right side encounters the same layer  $a$  in the case of sequences  $S'_k$ , whereas in the case of sequences  $S_k$  it may encounter either the

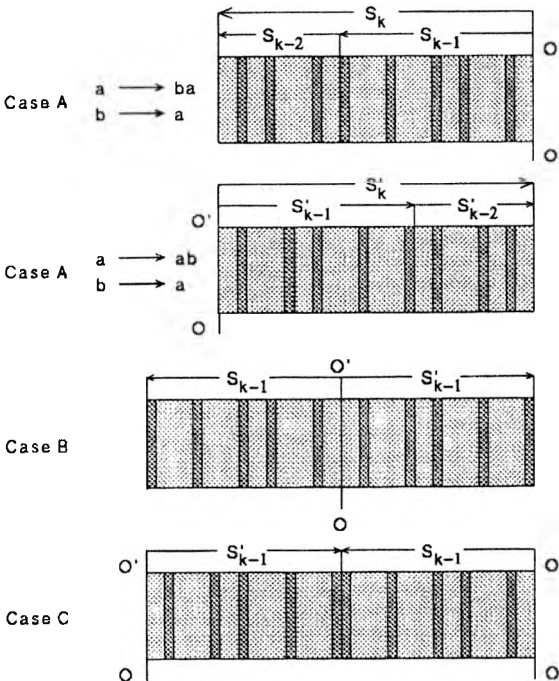


Fig. 1. Illustrations of F and FFP quasi-periodic sequences. Brighter and darker regions represent layers  $a$  and  $b$  of refractive indices  $n_1$  and  $n_2$ , respectively, with  $n_1 < n_2$ . The two sequences  $S_k$  and  $S'_k$  from the upper side (case A) are sets  $F$  at stage  $k = 7$  that are generated by transformations  $a \rightarrow ba$ ,  $b \rightarrow a$  and  $a \rightarrow ab$ ,  $b \rightarrow a$ , respectively.  $OO'$  is the starting line. Cases B and C represent FFP sequences obtained by arrangements  $\{S_{k-1}S'_{k-1}\}$  and  $\{S'_{k-1}S_{k-1}\}$ , respectively.

layer  $a$  or the layer  $b$ , e.g., it encounters the layer  $a$  if  $k = 2$  and the layer  $b$  if  $k = 3$ . With sequences  $S_{k-1}$  and  $S'_{k-1}$  one may generate two FFP sets, as shown in Fig. 1: the set  $\{S_{k-1}S'_{k-1}\}$  in case B and the set  $\{S'_{k-1}S_{k-1}\}$  in case C. In case B, sequences  $S_{k-1}$  and  $S'_{k-1}$  have the same starting line  $OO'$  which is in the centre of the set, whereas in case C the starting lines  $OO'$  are symmetrical with respect to the centre of the set. FFP sets of cases B and C resemble the positive and negative thick lenses, respectively. In all cases A, B and C, we assume that the multilayers are embedded in a medium of refractive index  $n_0$ .

Let us denote  $M_i$ , with  $i = 1, 2$ , the transfer matrices [10] of layers  $a$  and  $b$ ,

$$M_i = \begin{bmatrix} \cos \varphi & \frac{\sin \varphi}{k_0 n_i} \\ -k_0 n_i \sin \varphi & \cos \varphi \end{bmatrix}, \quad i = 1, 2 \quad (1)$$

where  $\varphi = k_0 L$  and  $k_0$  is a vacuum wave number. Let  $M^{(k)}$  and  $M'^{(k)}$  be the transfer matrices of sets  $S_k$  and  $S'_k$ , respectively. For  $k \geq 2$  they obey the recurrent relations:

$$M^{(k)} = M^{(k-1)}M^{(k-2)}, \quad (2a)$$

$$M'^{(k)} = M'^{(k-2)}M'^{(k-1)}, \quad (2b)$$

with  $M^{(0)} = M'^{(0)} = M_2$  and  $M^{(1)} = M'^{(1)} = M_1$ . The overall transfer matrix  $\mathfrak{N}^{(k)}$  is:

$$\mathfrak{N}^{(k)} = M^{(k)} \text{ in case A,}$$

$$\mathfrak{N}^{(k)} = M'^{(k-1)}M^{(k-1)} \text{ in case B,}$$

$$\mathfrak{N}^{(k)} = M^{(k-1)}M'^{(k-1)} \text{ in case C.}$$

### 3. Transmission properties

The complex amplitude transmission coefficient  $t_k$  for a multilayer having the transfer matrix  $\mathfrak{N}^{(k)}$  is given by

$$t_k = \frac{2}{\mathfrak{N}_{22}^{(k)} - \frac{\mathfrak{N}_{21}^{(k)}}{jk_0 n_0} - jk_0 n_0 \mathfrak{N}_{12}^{(k)} + \mathfrak{N}_{11}^{(k)}} \quad (3)$$

where  $j$  is an imaginary unit and  $\mathfrak{N}_{lm}^{(k)}$  ( $l, m = 1, 2$ ) are the elements of  $\mathfrak{N}^{(k)}$ . In all cases A, B, and C,  $|t_k|$  is a periodic function of  $\varphi$  with the period  $\varphi = \pi$ . It is symmetric with respect to  $\varphi = \pi/2$ .

Further on we give some numerical examples for the common material pair  $\text{SiO}_2/\text{TiO}_2$  that is used in the multilayer interference film industry [11], [12] with

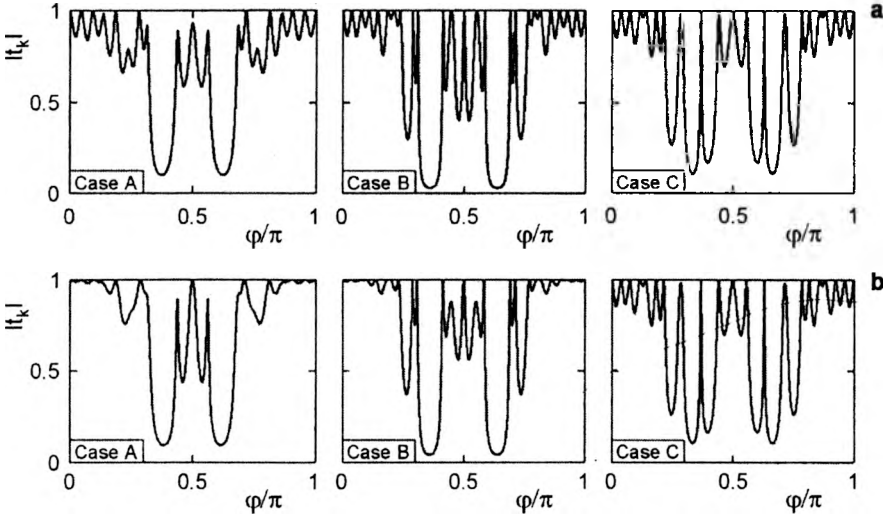


Fig. 2. Variations of  $|t_k|$  against  $\varphi/\pi$  in cases A, B and C, when  $n_1 = 1.46$  and  $n_2 = 2.4$  at  $n_0 = 1$  (a) and  $n_0 = 1.5$  (b);  $\varphi/\pi$  is varied in steps of 0.0005.

refractive indices  $n_1 = 1.46$  and  $n_2 = 2.4$ . The variation of  $|t_k|$  is plotted against  $\varphi/\pi$  in Figs. 2a and b, when  $n_0 = 1$  (air) and  $n_0 = 1.5$  (glass), respectively. There is a structured part with isolated peaks inside either forbidden gap. The gap is deeper and the structured central part is wider in case B. In case C the whole gap is structured with isolated peaks.

It has been shown in [4] that at  $\varphi/\pi = 1/2$  the transfer matrix of the sequence F has a period of six, that is,  $\mathfrak{M}^{(k)} = \mathfrak{M}^{(k+6)}$  for any value of  $k$ . Thus, at  $\varphi/\pi = 1/2$ , in case A,  $\mathfrak{M}^{(7)} = \mathfrak{M}^{(1)} = M_1$  and the sequence F behaves like a quarterwave-thick layer of refractive index  $n_1$ , with the magnitude of the transmission coefficient

$$|t_{kc}| = \frac{2n_0n_1}{n_0 + n_1}. \quad (4)$$

Thus, the magnitude of transmission at the centre of the spectrum in case A does not depend on  $n_2$ , and is greater for  $n_0 = 1.5$  than for  $n_0 = 1$ , as may be seen in the respective subplots of Figs. 2. In cases B and C, at  $\varphi/\pi = 1/2$ , the FFP sets behave like a halfwave-thick layer, and thus  $|t_{kc}| = 1$  for any value of  $n_0$ ,  $n_1$  and  $n_2$ , as can be seen in Figs. 2.

#### 4. Temporal pulse response

In what follows the pulse amplitude in the time domain will be denoted by the lower case letter  $x$  while the capital letter  $X$  will be used to represent the respective Fourier transform. Consider an input Gaussian temporal pulse of the form

$$x_{\text{in}} = x_0 \exp[-(t/\tau)^2] \quad (5)$$

where  $x_0$  is the pulse peak amplitude and  $2\tau$  is the full pulse width at the  $\exp(-1)$  level. The frequency spectrum of this input pulse is also a Gaussian function that is centred in the middle of the gap. Since  $t_k$  represents the transfer function for a multilayer, upon the completion of the Fourier transform we determine the amplitude of the transmitted pulse for each Fourier component. The frequency-domain output pulse is then reconstructed in the time domain through the inverse Fourier transform. We consider an optimal situation when the frequency spectrum of the input pulse is wide enough to cover the isolated, structured central part inside the gap. Thus, we choose  $\tau = 5$ . Output time-domain pulses are shown in Fig. 3 in cases A, B and C, at  $n_0 = 1$ . Like Cantor filters [9], the F and FFP filters exhibit a compression behaviour: the output time-domain pulse is narrower, especially in case B than the input Gaussian pulse that is shown for comparison in Fig. 3 by a dotted line.

To characterise the compressing capacity we use three parameters [9]:

- the compression ratio (CR), that is, the ratio between the widths at half height of the input and output pulses;
- the amplitude ratio (AR), that is, the ratio between the peak amplitudes of the output and input pulses;
- the compression efficiency (CE), that is the product of CR and AR.

The behaviour of AR for different pairs  $(n_1, n_2)$  of the layer refractive indices, for the same optical thickness  $L$ , is shown in Fig. 4, when  $n_0 = 1$ , in case B. If  $n_2$  has a fixed value,  $n_2 = 2.3$ , AR increases when  $n_1$  takes values from 1.3 to 2, as can be seen

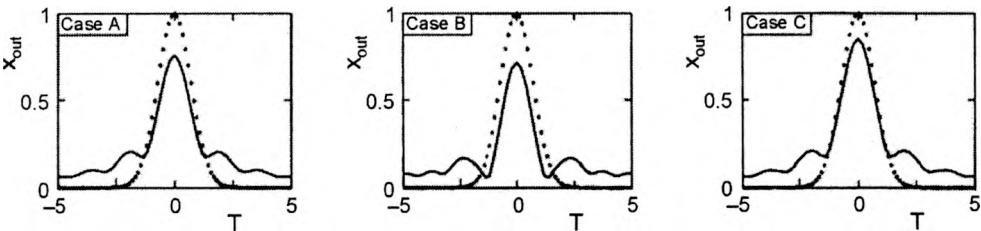


Fig. 3. Amplitude  $x_{out}$  of the time-domain output pulse against  $T = t/\tau$  in cases A, B, and C, when  $n_0 = 1$ ,  $n_1 = 1.46$  and  $n_2 = 2.4$ . For comparison, the input Gaussian time-domain pulse is represented by dotted lines.

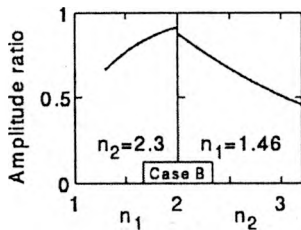


Fig. 4. Amplitude ratio in case B, when  $n_2 = 2.3$  and  $n_1$  takes values from 1.3 to 2 (first part), and when  $n_1 = 1.46$  and  $n_2$  takes values from 2 to 3.2 (second part), at  $n_0 = 1$ . Refractive indices are varied in steps of 0.01.

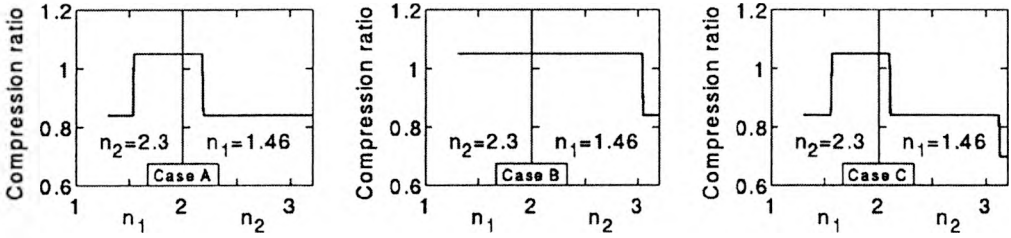


Fig. 5. Compression ratio in cases A, B and C, when  $n_2 = 2.3$  and  $n_1$  takes values from 1.3 to 2 (first part in either case), and when  $n_1 = 1.46$  and  $n_2$  takes values from 2 to 3.2 (second part in either case), at  $n_0 = 1$ . Refractive indices are varied in steps of 0.01.

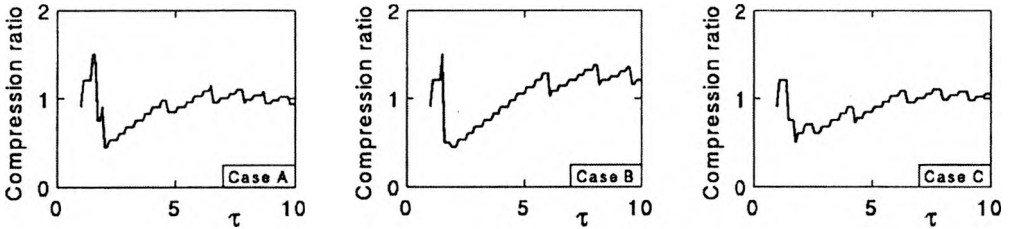


Fig. 6. Compression ratio against  $\tau$  in cases A, B, and C, when  $n_0 = 1$ ,  $n_1 = 1.46$ , and  $n_2 = 2.4$ ;  $\tau$  is varied in steps of 0.1.

in the first part of Fig. 4. If  $n_1$  has a fixed value,  $n_1 = 1.46$ , AR decreases when  $n_2$  takes values from 2 to 3.2, as one can see in the second part of Fig. 4. The behaviour of AR in cases A and C is similar to that in case B. The behaviour of CR for different pairs  $(n_1, n_2)$  of the layer refractive indices, for the same optical thickness  $L$ , is shown in cases A, B, and C in Fig. 5, when  $n_0 = 1$ . It is remarkable that in case B, CR is constant over a wide interval of  $n_1$  and  $n_2$  variation. Thus, if  $n_2$  has a fixed value,  $n_2 = 2.3$ , CR in case B is constant when  $n_1$  takes values from 1.3 to 2, whereas if  $n_1$  has a fixed value,  $n_1 = 1.46$ , CR in case B is constant when  $n_2$  takes values from 2 to 3. The behaviour of CE for different pairs  $(n_1, n_2)$  of the layer refractive indices is similar to that of AR.

For the sake of completeness, variation of CR against  $\tau$  is shown in Fig. 6, in cases A, B and C, for  $n_0 = 1$ . The maximum of CR is at  $\tau = 1.3$ , but for this value of  $\tau$  the frequency spectrum of the input pulse may extend over the gap at some values of  $n_1$  and  $n_2$ . The train of time-domain output pulses is anyway characterised by a central intense pulse that can be shorter than the input pulse, but the first lateral pulses around the central pulse in the train may have an amplitude higher than one half of the central amplitude.

Note that, compared to a Cantor set of almost the same overall optical thickness [9], CR is smaller, but AR is greater in the case of F and FFP sets, and this is because the structured part with isolated peaks inside the gap is wider in the case of F and FFP sets than in the case of Cantor sets.

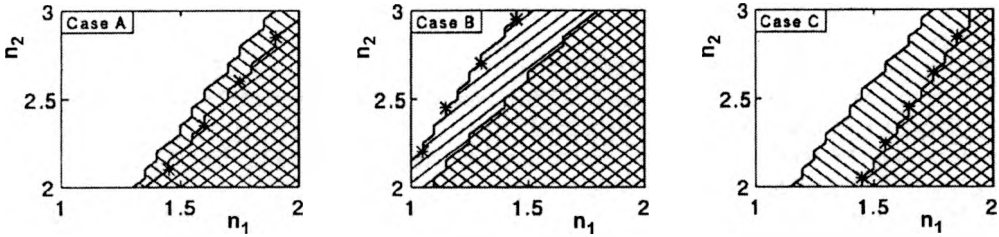


Fig. 7. Diagrams showing the pairs  $(n_1, n_2)$  at which  $CR \geq 1$  (hatched region bordered by the curve marked with asterisks) and  $CE \geq 0.6$  (region hatched at opposite slope) in cases A, B and C, at  $n_0 = 1$ . In the overlapping (double-hatched) regions both conditions for CR and CE are fulfilled;  $n_1$  and  $n_2$  are varied in steps of 0.05.

Diagrams of Fig. 7 show the pairs  $(n_1, n_2)$  of the layer refractive indices at which parameters CR and CE that characterise the compressing capacity attain specified levels in cases A, B and C, by assuming the same optical thickness  $L$ , when  $\tau = 5$  and  $n_0 = 1$ . From Fig. 7 we see that regions of  $(n_1, n_2)$  values are considerably wider in case B. One can also see that, at some fixed value of  $n_1$ , the smaller the  $n_1$  is, the narrower the interval of  $n_2$  values at which CR and CE attain the specified levels, whereas at fixed value of  $n_2$ , the smaller the  $n_2$  is, the wider the interval of  $n_1$  values at which CR and CE attain the specified levels. Note that in case B, the regions of  $(n_1, n_2)$  values at which CR and CE attain the specified levels are wider when  $n_0 = 1.5$  than when  $n_0 = 1$ .

## 5. Summary

Recent advances in the technologies of film synthesis make it possible to realise different values of the layer refractive indices for various pairs of optical materials [11], [12]. The paper presents an analysis of the temporal pulse response from quasi-periodic F and FFP multilayers that are shown in Fig. 1, for various pairs  $(n_1, n_2)$  of nondispersive layer refractive indices and different embedding media, at normal incidence. The optimal situation is chosen when the frequency spectrum of the Gaussian input pulse, that is centred in the middle of the gap, is wide enough to cover the isolated peaks existing inside the gap. The results show that the symmetrical FFP sequence of case B admits wider intervals of refractive indices at which the parameters characterising the compressing capacity attain specified levels. These results may be useful in the design of nonlinear multilayers for optical limiting and switching of short pulses [7], [8].

## References

- [1] LARUELLE F., ETIENNE B., Phys. Rev. B **37** (1988), 4816.
- [2] RIKLUND R., SEVERIN M., J. Phys. C: Solid State Phys. **21** (1988), 3217.
- [3] BERTOLOTTI M., MASCIULLI P., SIBILIA C., Opt. Lett. **19** (1994), 777.
- [4] GELLERMANN W., KOHMOTO M., SUTHERLAND B., TAYLOR P.C., Phys. Rev. Lett. **72** (1994), 633.

- [5] BERTOLOTTI M., MASCIULLI P., SIBILIA C., WIJNANDS F., HOEKSTRA H., *J. Opt. Soc. Am. B* **13** (1996), 628.
- [6] SIBILIA C., NEFEDOV I.S., SCALORA M., BERTOLOTTI M., *J. Opt. Soc. Am. B* **15** (1998), 1947.
- [7] SCALORA M., DOWLING J.P., BOWDEN C.M., BLOEMER M.J., *Phys. Rev. Lett.* **73** (1994), 1368.
- [8] TRAN P., *J. Opt. Soc. Am. B* **14** (1997), 2589.
- [9] GARZIA F., MASCIULLI P., SIBILIA C., BERTOLOTTI M., *Opt. Commun.* **147** (1998), 333.
- [10] LEKNER J., *J. Opt. Soc. Am. A* **11** (1994), 2892.
- [11] WEBER M.F., STOVER C.A., GILBERT L.R., NEVITT T.J., OUDERKIRK A.J., *Science* **287** (2000), 2451.
- [12] WANG X., MASUMOTO H., SOMENO Y., HIRAI T., *Appl. Phys. Lett.* **72** (1998), 3264.

*Received November 12, 2001*